# Interim Report for Phase II – Task 4 of the Comprehensive Study to Understand Longitudinal ERW Seam Failures

## "Models and Mechanisms with Validation Results"

Authors

Richard Olson, Bruce A. Young, and Jennifer M. O'Brian

Battelle Memorial Institute
505 King Avenue
Columbus, OH 43201

Prepared for

U.S. Department of Transportation
Pipeline and Hazardous Materials Safety Administration
1200 New Jersey Ave., SE
Washington DC 20590

Contract No. DTPH56-11-T-000003
Battelle Contract No. G006084
Battelle Project No. 100004552

May 2017

Battelle does not engage in research for advertising, sales promotion, or endorsement of our clients' interests including raising investment capital or recommending investments decisions, or other publicity purposes, or for any use in litigation.

Battelle endeavors at all times to produce work of the highest quality, consistent with our contract commitments. However, because of the research and/or experimental nature of this work the client undertakes the sole responsibility for the consequence of any use or misuse of, or inability to use, any information, apparatus, process or result obtained from Battelle, and Battelle, its employees, officers, or Directors have no legal liability for the accuracy, adequacy, or efficacy thereof.

© 2017 Battelle
This publication may not be reproduced or distributed without the prior written permission of the copyright owner.

# Acknowledgments

Useful discussions during this phase of the project with B.N. Leis of B.N. Leis, Inc. are acknowledged.

## Executive Summary

On November 1, 2007 a liquid propane pipeline operated by Dixie Pipeline Company ruptured near Carmichael, Mississippi, which several pipeline industry experts collaboratively indicated the origin was likely a defect in the longitudinal ERW seam, with the ensuing fracture running along that joint into portions of the adjacent pipes. These experts also noted that a seam-integrity assessment did not prevent the failure, as this failure came 2 years after an in-line inspection (ILI) with a sophisticated crack-detection tool; and 23 years after a hydrostatic test to a hoop stress level greater than 1.25 times the maximum operating hoop stress level. Following the NTSB's public report, the NTSB issued Recommendation P-09-1, which called upon the PHMSA to conduct a comprehensive study to identify actions that can be used by operators to eliminate catastrophic longitudinal seam failures in pipe, and indicated the required scope. This led to the PHMSA issued a research announcement (RA) that targeted Recommendation P-09-1 in the form of BAA Solicitation DTPH56-11-RA-000001. That Solicitation sought a Comprehensive Understanding of Longitudinal ERW Seam Failures.

In response to that Solicitation, Battelle, as the prime contractor, proposed a two-phase project to work to develop the understanding sought by the research announcement in resolving Recommendation P-09-1.

The Phase I final report was issued in January 2014 and can be found at the following website: https://primis.phmsa.dot.gov/matrix/PrjHome.rdm?prj=390. Phase II has five tasks including:

- Task 1: Hydrotest protocols
- Task 2: ILI and ITDM Inspection Assessment
- Task 3: Defect Characterization: Types, Sizes, Shapes, and Idealizations
- Task 4: Model Validation
- Task 5L: Software Development for Integrity Management of Long Seam Welds.

This report focuses on the results obtained during the work completed under Phase II, Task 4 which includes the development and refinement of the of the analytical

models used to define crack growth and failure. The results of this task are implemented in the software development task (Task 5).

## Contents

Acknowledgments ..... iii

Executive Summary ..... iv

Acronyms and Nomenclature ..... vii

Introduction ..... 9

Phase II, Task 4 ..... 9

Models ..... 9

- Time-Independent Failure Prediction Models ..... 10
- Time-Dependent Failure Prediction Models ..... 14

Validation ..... 25

- Time-Independent Models ..... 25
- Time-Dependent Models ..... 26

Conclusions and Recommendations ..... 47

Works Cited ..... 48

## List of Figures

Figure 1. Typical X52 grade pipe steel stress-strain behavior ..... 13
Figure 2. Typical X52 grade pipe steel J-R curve behavior with CVN= 43.4 N-m ..... 13
Figure 3. Evolution of Ramberg-Osgood parameter α as a function of time for a typical X52 grade pipe steel ..... 17
Figure 4. Evolution of Ramberg-Osgood parameter n as a function of time for a typical X52 grade pipe steel ..... 18
Figure 5. Typical effect of time variation of α and n for an X52 grade steel ..... 18
Figure 6. Comparison of short-term J-integral values for a cracked center cracked panel at three levels (295.6, 322.7, 358.5 MPa) ..... 19
Figure 7. Comparison of long-term J-integral values for a cracked center cracked panel at three levels (295.6, 322.7, 358.5 MPa) ..... 19
Figure 8. Generic fatigue crack growth behavior [12] ..... 21
Figure 9. Typical crack growth transients around an overload [10] ..... 24
Figure 10. Willenborg crack retardation model plastic zone [10] ..... 24
Figure 11. Pressurization data for time-dependent growth hydrotest model validation ..... 31
Figure 12. Observed and predicted time-dependent flaw growth for a 7.00 mm x 133.86 mm surface flaw in 762 mm x 10 mm X52 pipe ..... 32
Figure 13. Observed and predicted time-dependent flaw growth for a 7.11 mm x 126.37 mm surface flaw in 762 mm x 10 mm X52 pipe ..... 32
Figure 14. Observed and predicted time-dependent flaw growth for a 7.57 mm x 120.65 mm surface flaw in 762 mm x 10 mm X52 pipe ..... 33
Figure 15. Observed and predicted time-dependent flaw growth for a 7.72 mm x 109.73 mm surface flaw in 762 mm x 10 mm X52 pipe ..... 33

Figure 16. Intensity Range Profiles for Grade B Tests ..... 34
Figure 17. Intensity Range Profiles for Grade X-70 Tests ..... 35
Figure 18. Unity Plot for Crack Sizes of the Grade B Tests ..... 35
Figure 19. Unity Plot for Crack Lengths of the X-70 Tests ..... 36
Figure 20. Cross Section of the Test Apparatus ..... 39
Figure 21. Picture of the Bottom Head and Hydraulic Actuator ..... 40
Figure 22. Picture of a Typical Test Flaw ..... 41
Figure 23. Picture of the Assembled Specimen ..... 42
Figure 24. Picture of the Specimen and Servo-Hydraulic Test Control System ..... 43
Figure 25. Post-test picture of the 0.040" deep x 0.800" long ..... 45

## Acronyms and Nomenclature

| | |
|---|---|
| PipeAssess PI™ | Battelle's Cracking Assessment for Pipeline Software |
| ERW | Electric Resistance Welded |
| ILI | Inline Inspection |
| SSWC | selective seam weld corrosion |
| $\sigma_u$ | ultimate tensile strength |
| CCP | center cracked panel |
| SEN | single edge notch |
| SIF | stress intensity factor |
| MOP | maximum operating pressure |
| $t$ | wall thickness |
| $D$ | pipe diameter |
| $d$ | flaw depth |
| $L$ | flaw length |
| $R_o$ | outside radius of the pipe |
| $t_o$ | net-section thickness (i.e., $t_o = (t - d)$ |
| $P$ | Pressure |
| $C_c$ | plastic collapse fitting constant |
| K | elastic stress intensity factor |
| J | J-integral |
| $J_{el}$ | elastic contribution to J |
| $J_{pl}$ | plastic contribution to J |
| $J_{app}$ | applied J |
| $J_{applied}$ | applied J |
| $J_{mat}$ | material resistance in terms of J |
| $J_{material}$ | material resistance in terms of J |
| $J_i$ | initiation J |
| A | crack depth |

| | |
|---|---|
| CVN | Charpy V-notch energy |
| J-R | curve of $J_{mat}$ versus $\Delta a$ |
| $C, m$ | J-R curve fitting coefficients |
| $\alpha, n$ | Ramberg-Osgood equation coefficients |
| $\varepsilon$ | Strain |
| $\sigma$ | Stress |
| $\sigma_0$ | Ramberg-Osgood reference stress |
| c, 2c | half and full crack length |
| $\tau$ | Time |
| $f$ | stress intensity crack geometry factor |
| $\Delta K$ | stress intensity factor range $=K_{max}-K_{min}$ |
| $\Delta K_{th}$ | stress intensity factor range threshold |
| R | stress ratio (min/max) |
| $\frac{da}{dN}$ | crack growth per cycle |
| N | number of cycles |

## Introduction

Work under Phase I followed a scope identified from National Transportation Safety Board (NTSB) Recommendation P-09-1 that developed understanding of longitudinal Electric Resistance Welded (ERW) seam failures by: 1) generating a database that quantified the industry and Government experience in regard to hydrotest and in-service failures, 2) completing a full-scale project that empirically quantified ERW seam failure behavior and resistance, and 3) developing technology to assess susceptibility to selective seam corrosion. Phase II builds on that understanding by establishing the viability of condition monitoring technology that relies on hydrotesting, in-line non-destructive inspection, and in-the-ditch nondestructive inspection along with the development of the engineering tools to translate condition into viable metrics of defect severity and re-inspection interval specific to ERW seam defects. Viability in all aspects will be assessed and demonstrated through use of full-scale burst tests that address the range of defects characteristics across that seen in the database developed in the initial phase of this of project. Management tools will be developed for use by pipeline operators as part of their integrity management plan to assure that their ERW pipelines are safe. This report focuses on the results obtained during the work completed under Phase II, Task 4.

## Phase II, Task 4

## Models

Loss of pressure integrity in transmission pipelines can occur by several mechanisms. Time-independent failure can occur by plastic collapse, also known as net-section collapse, or it can occur by fracture, which can be brittle or ductile. Likewise, time-dependent failure can occur by stress-induced creep or it can occur by fatigue. Comprehensive assessment of pipeline integrity, which includes the effects of sustained static loading, hydrotesting, and cyclic pressure loading, requires consideration of all these loading types for safe operation.

ILI inspections can identify and size defects, but size by itself does not define defect tolerance or limiting pressure capacity. For this, models driven by ILI crack size

and relevant pipeline steel material properties are needed. In the following section, the various models incorporated in PipeAssess PI™ are described.

## Time-Independent Failure Prediction Models

Time-independent failure of an axially cracked pipeline can occur by either plastic collapse or by fracture. Because both plastic collapse and fracture mechanisms can limit the pressure capacity or defect tolerance of a pipeline, applicable models must address both possibilities, with failure being due to the mechanism that leads to the lowest predicted failure pressure.

### *Plastic Collapse*

Plastic collapse occurs in a pipeline with axial cracks when the remaining ligament from the bottom of the crack to the pipe wall is insufficient to sustain the applied tensile hoop stress. In its simplest form, the plastic collapse pressure for an axially cracked pipe can be taken as simple equilibrium of remotely applied hoop stress with a stress called flow stress (conventionally the average of yield and ultimate) over the pipe wall thickness less the crack depth [1]. This is the basic idea behind the plastic collapse or reference stress solutions found in Fitness-for-Service codes such as API-579 [2] or BS-7910 [3]. As flaw integrity evaluations have evolved, finite element analysis techniques have matured, and data for burst tests of high CVN pipe have been developed, the simple hoop-flow stress equilibrium model has been replaced by less conservative models specifically tuned for pipeline failure problems.

In the mid 1990s, work was underway to develop a general plastic-collapse-based solution for blunt metal-loss defects such as corrosion [4] [5]. This work determined that failure via plastic collapse occurred at or near the ultimate tensile strength of the pipeline material, rather than at flow stress, as the simple equilibrium model assumes. The collapse-based failure pressure for blunt metal-loss has the form [4] [5]:

$$P = \sigma_u \frac{2t}{D}\left\{1 - \frac{d}{t}\left[1 - exp\left(C_c \frac{L}{\sqrt{R_o t_o}}\right)\right]\right\} \tag{1}$$

where

$\sigma_u$ ultimate tensile strength

| | |
|---|---|
| $t$ | wall thickness |
| $D$ | pipe diameter |
| $d$ | flaw depth |
| $L$ | flaw length |
| $R_o$ | outside radius of the pipe |
| $t_o$ | the net-section thickness (i.e., $t_o = (t - d)$ |
| $C_c$ | a constant determined as -0.157 by best-fitting FEA results for corrosion-thinned pipelines. |

Accurate predictions of full-scale testing of corroded pipe with this approach led to the formulation of an analogous plastic collapse solution for sharp defects relevant to higher-toughness pipeline applications, for which initially sharp defects blunt prior to fracture initiation. Thus, Equation (1**)**, with a different constant $C_c$, derived from finite element analyses of sharp defects, can be used for plastic collapse of axially cracked pipes.

Plastic collapse failures are instantaneous: There simply is not enough material left in the cracked section to carry the applied stress. Furthermore, plastic collapse failure is independent of the pipe steel toughness, so long as the material has enough toughness to preclude a fracture mechanism failure.

### *Brittle Failure and Tearing*

A second time-independent failure mechanism for axially cracked pipes is a fracture mechanics brittle or tearing failure. Typically, brittle failure is characterized by the stress intensity factor, K, and the tearing failure is characterized by the J-integral which represents the strain energy release rate, or work (energy) per unit fracture surface area in a material. In the limit, brittle behavior and tearing behavior can coalesce into a single J-controlled model for prediction of axially cracked pipe failure pressure. A J-controlled failure is a progressive failure in which material strength and toughness determine whether a crack will initiate and grow. Such growth, when it occurs, results in a crack that eventually reaches a critical state. i.e. rupture.

Ductile crack growth in line-pipe materials is assumed to be J controlled, wherein.the J-integral is used to describe the stress singularity at the crack-tip for elastic–plastic hardening materials like line pipe steels. J is the direct analog of the stress

intensity factor K that is used to characterize the intensity of a crack singularity in a linear elastic stress field in brittle materials. In J space, the driving force for extending a crack, $J_{applied}$, is a function of the applied stress, current pipe/crack geometry and plasticity of the pipe steel. Resistance to crack extension, $J_{material}$, is controlled by the steel's toughness. Depending on the magnitudes and rates of change of $J_{applied}$ and $J_{material}$, cracks may simply not initiate, they may grow then arrest, or they may grow unstably, i.e. fail.

In simplified terms, $J_{applied}$ can be divided into an elastic and plastic contribution,

$$J_{app} = J_{el} + J_{pl} \tag{2}$$

where $J_{el}$ is calculated using standard elastic stress intensity factor solutions. $J_{pl}$ is a function of the nonlinear stress-strain behavior of the material, the size of the plastic zone ahead of the crack, crack size, pipe geometry, and the applied stress. As is typical for ductile tearing problems, the nonlinear material stress-strain response is assumed to follow the Ramberg-Osgood model [6],

$$\frac{\epsilon}{\epsilon_0} = \frac{\sigma}{\sigma_0} + \alpha\left(\frac{\sigma}{\sigma_0}\right)^n \tag{3}$$

Also typical for ductile tearing problems, material resistance (toughness) is assumed to take the following form,

$$J_{mat} = J_i + C(\Delta a)^m \tag{4}$$

where $J_i$ is the initiation toughness, C is a toughness modulus and m is a toughness exponent. The curve defined by Equation (4) is called a J-resistance or J-R curve. J-R curves are not usually generated for pipeline steels, but Charpy V-notch energies (CVN) are, so correlations are used to convert Charpy energy into J-R curves. At the extreme of low CVN toughness, Equations (4) and (2) will yield brittle behavior.

Figure 1 and Figure 2 show typical pipeline X52 grade steel stress-strain and J-resistance (toughness) curves.

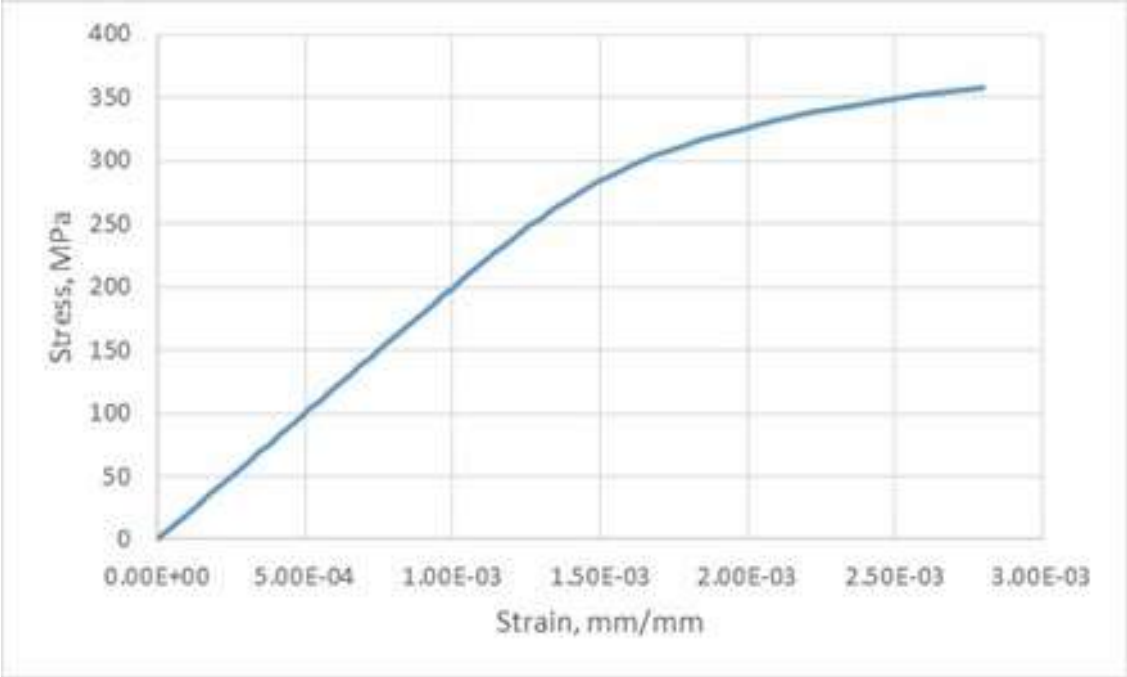


**Figure 1. Typical X52 grade pipe steel stress-strain behavior**

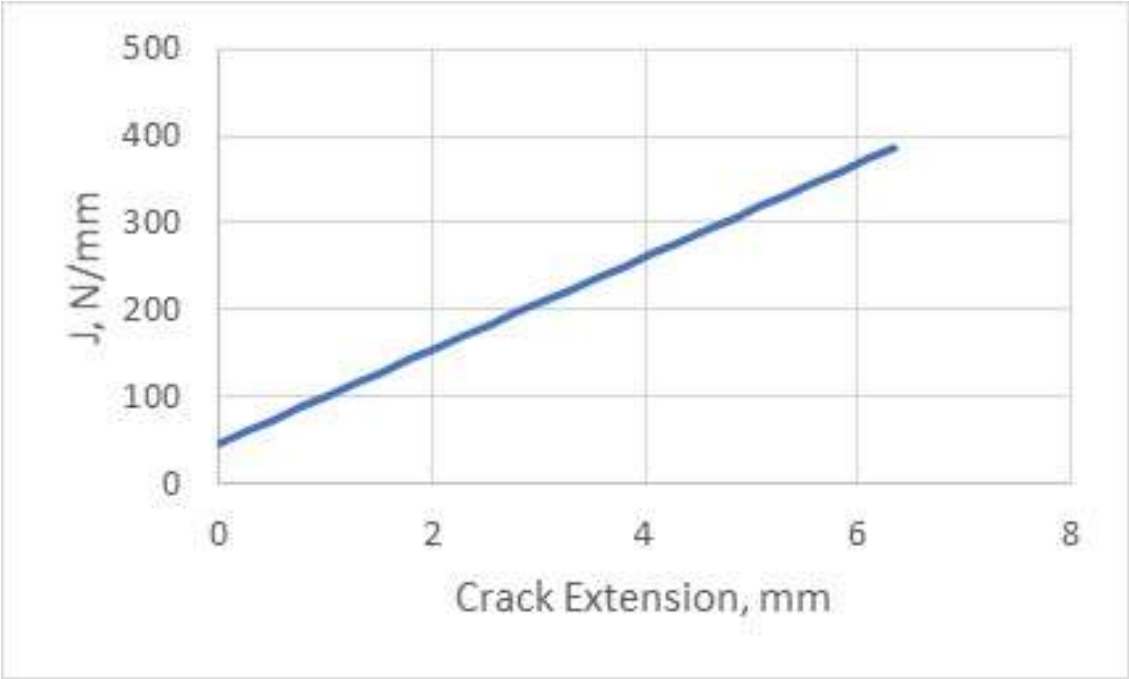


**Figure 2. Typical X52 grade pipe steel J-R curve behavior with CVN= 43.4 N-m**

During a straightaway pressure to failure test in a pipe with axial cracks where the pressure is applied quasi-statically, for some pressure (hoop stress), if $J_{applied}$ is less than

$J_i$, a crack will not initiate or grow. If $J_{applied}$ is greater than $J_i$, crack growth will occur to maintain the condition $J_{applied}=J_{material}$. Whether such crack growth causes the crack to become unstable is expressed by the rate of change of J inequality,

$$\frac{dJ_{app}}{da} > \frac{dJ_{mat}}{da} \tag{5}$$

Thus, given appropriately small quasi-static increments in pressure and assuming pressure always increases, crack growth will be initiated at some pressure and then the crack will grow until it eventually reaches the condition given in Equation (5). The rate of crack growth is always increasing as the pressure goes up because the crack is getting ever bigger. In the global time domain, however, growth and instability are virtually instantaneous, that is, tearing failures, whether brittle or ductile, are considered to be time-independent.

The root constituents for the failure model described above are the elastic stress intensity factor and its associated plastic zone size. Through a reasoned set of facture mechanics arguments and the known relationship between K and J, an expression for $J_{pl}$ can be developed, where the plastic contribution to J is a function of the Ramberg-Osgood parameters, among other things. Coupled with the elastic contribution $J_e$ to $J_{app}$ directly from K, $J_{app}$ can be calculated and the critical pressure when Equation (5) and $J_{applied}=J_{material}$ are satisfied can be found iteratively.

The efficacy of the basic J-tearing solution for longitudinal surface cracks in pipes described above has been confirmed by comparison against finite element analyses and comparison with pipe rupture experiments [7]. As long as the CVN is low enough to exclude the possibility of a plastic collapse failure, tearing (brittle or ductile) will be the failure mode of axially cracked pipes.

## Time-Dependent Failure Prediction Models

Part of pipeline integrity management includes hydrostatic pressure tests that are performed during commissioning. As pipelines age, hydrotests are also used to revalidate integrity. Notionally, the hydrotest is designed to cause all longitudinal surface crack

defects that could subsequently fail during operational pressure cycles to go through wall. In addition, for remaining sub-critical flaws, another desired effect of a hydrotest is to induce a plastic zone in front of cracks that will impede future fatigue crack growth. The counter desire is to limit the flaw growth during hydrotesting so that existing flaws will not become critical over the same operational time.

From practical experience, hydrotest failures of pipeline defects (leaks) do not always happen as the pipeline is being pressurized. Rather, in many cases the pipeline ruptures minutes to hours to tens of hours after the test pressure has been attained and held steady. This time-dependent behavior suggests that there is some sort of stress-induced room-temperature creep mechanism going on.

In addition to hydrotests, pipelines also undergo cyclic fatigue due to pressure variations. Such pressure variations are caused by pipeline throughput variations, changes in pumped product, and thermal effects, and may range from trivial pressure variations to swings as large as MOP down to shut-in (essentially zero pressure). As a consequence of the pressure variations, existing cracks may grow, they may grow and blunt, or they may be completely unaffected. Interaction does exist between fatigue and hydrotests in that instantaneous crack size and size of the plastic zone ahead of the crack influence subsequent crack evolution from hydrotest to fatigue and back.

Both the hydrostatic test scenario (stress-induced creep) and fatigue crack growth are time-dependent phenomena. Hydrotests, typically, have a time scale of only hours, while fatigue occurs on a time scale of the life of the pipeline (years). In any event, to be able to predict expected remaining life or to be assured of pipeline integrity over some window of time, both time-dependent failure mechanisms must be modeled.

### *Stress-Induced Creep*

At some level of consideration, a hydrostatic test behaves identically to a J-tearing failure, except that the J-tearing failure has no provision for time dependency: The crack either grows or it doesn't, the pipe either ruptures or it doesn't. By adding a temporal element to the basic J-tearing failure, however, a hydrotest can be modeled as a simple extension to the J-tearing failure model. The resulting time-dependent crack growth can be characterized as stress-induced creep. Significant crack growth can occur during

hydrostatic pressure hold periods, so neglecting stress-induced creep time-dependent effects would be non-conservative.

Examining the possibilities for making the J-tearing failure exhibit time-dependent behavior, one could either consider the strength properties (Ramberg-Osgood parameters) to change with time, or one could consider the toughness (J-R curve) to degrade with time. Either possibility could work, but tests on compact tension experiments have shown that load-hold effects at room temperature to 250C conditions have almost no effect on the J-R curve [8]. Accordingly, changing the J-R curve with time does not seem technically justified. Thus, to model the creep behavior observed in hydrotests, Equation (1) was assumed to take the revised form,

$$J_{app} = J_{el} + J_{pl}(\tau) \tag{6}$$

where the plastic contribution to $J_{app}$ is now taken to be a function of time by re-writing Equation (3) as,

$$\frac{\epsilon}{\epsilon_0} = \frac{\sigma}{\sigma_0} + \alpha(\tau)\left(\frac{\sigma}{\sigma_0}\right)^{n(\tau)} \tag{7}$$

Figure 3 shows how $\alpha$ evolves with time and Figure 4 shows how $n$ changes with time for an X52 grade pipe. The $\alpha$ and $n$ changes result in typical stress-strain differences shown in Figure 5. The plastic contribution to J is a function of the Ramberg-Osgood parameters, so, as time passes during a hydrostatic pressure hold, $J_{app}$ changes, crack growth may occur subject to the $J_{applied}$=$J_{material}$ requirement, and instability may will occur subject to the Equation (5) condition.

Using a proper strain-rate dependent creep model and isochronous stress-strain curve data, detailed finite element calculations were performed to compare with the simplified engineering creep model defined by Equation (6) for single edge notch (SEN) and center cracked panel (CCP) geometries. Figure 6 and Figure 7 show a comparison of the CCP results for J as a function of time at three different applied stress levels [7]. The

simplified J-based engineering model is remarkably accurate. (See Validation Section for comparison of the model to test data)

During simulation of a hydrotest event, the crack plastic zone size at the end of the hydrotest is always calculated and saved for future use in subsequent fatigue crack growth calculations that incorporate a fatigue crack growth rate threshold stress intensity factor (SIF) to account shut-off of crack growth below a certain SIF value, a Walker model [9] to account for variations in stress-ratio effect, and a Willenborg model [10] to account for the retardation in growth rates after a stress over-load.

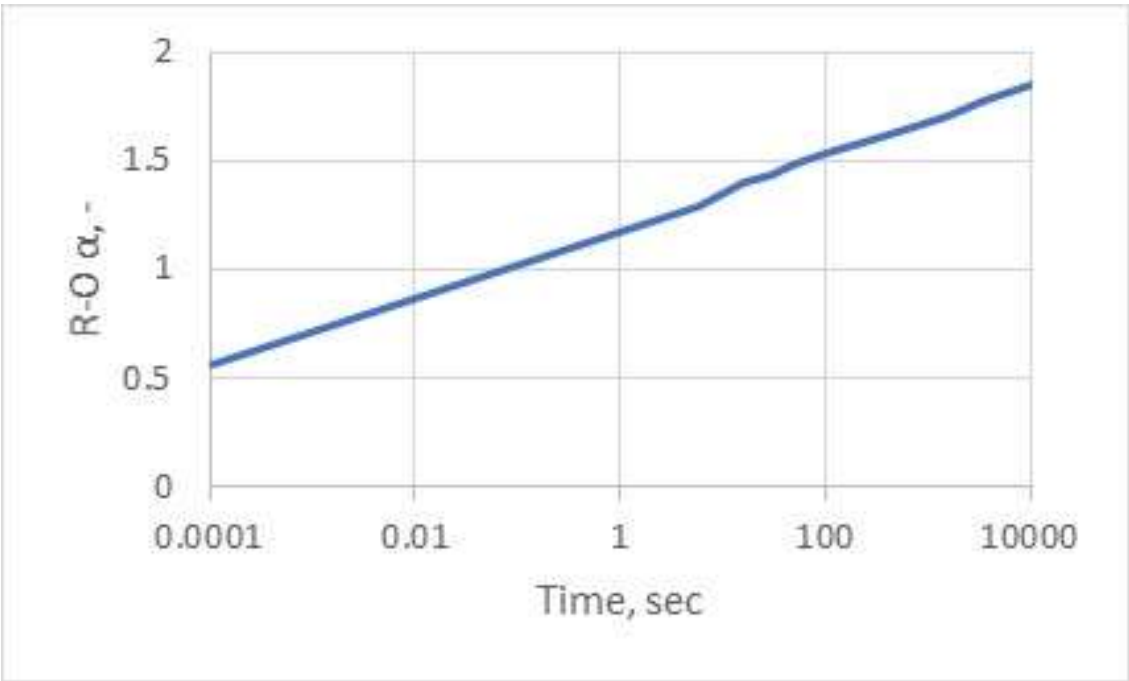


**Figure 3. Evolution of Ramberg-Osgood parameter α as a function of time for a typical X52 grade pipe steel**

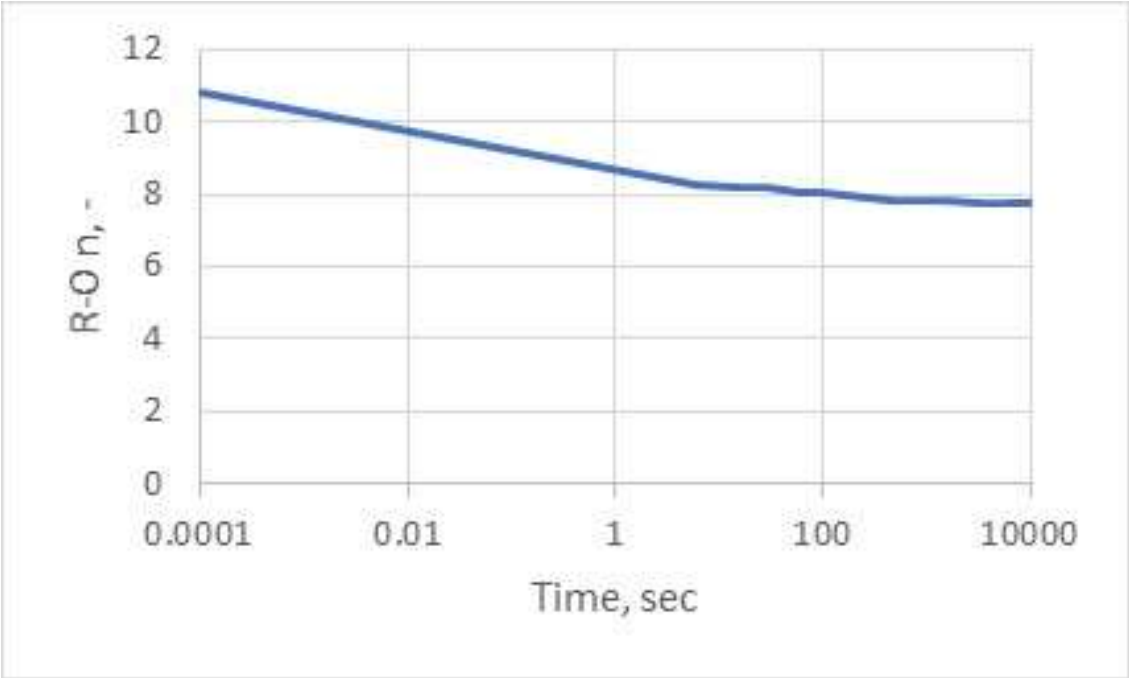


**Figure 4. Evolution of Ramberg-Osgood parameter n as a function of time for a typical X52 grade pipe steel**

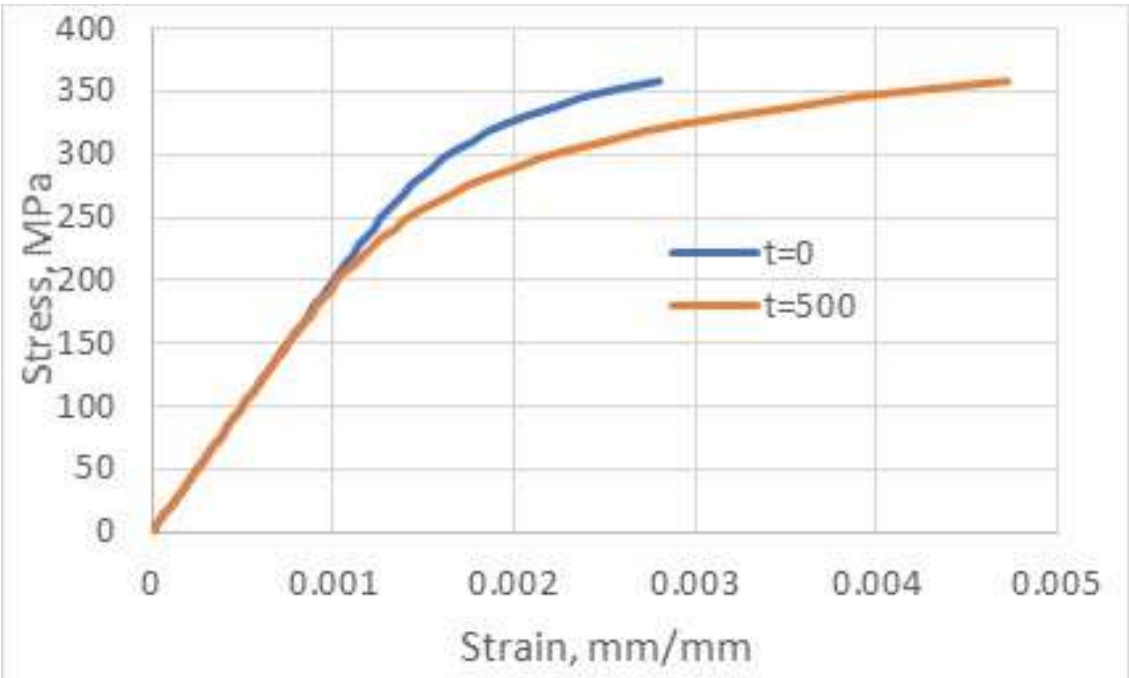


**Figure 5. Typical effect of time variation of α and n for an X52 grade steel**

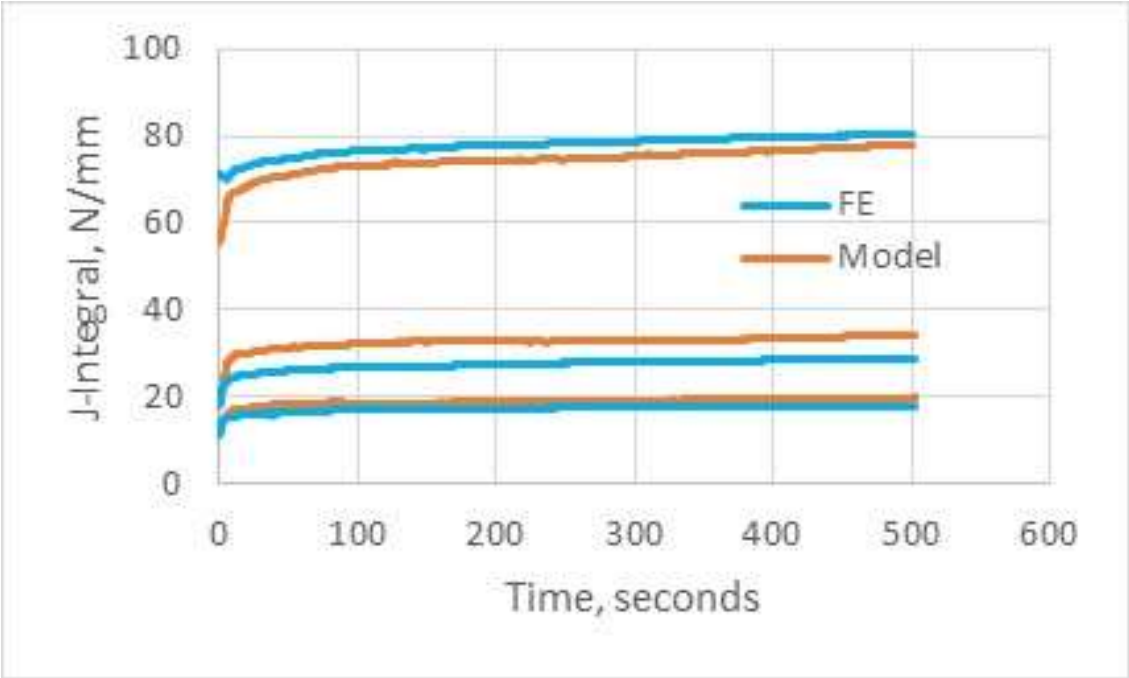


**Figure 6. Comparison of short-term J-integral values for a cracked center cracked panel at three levels (295.6, 322.7, 358.5 MPa)**

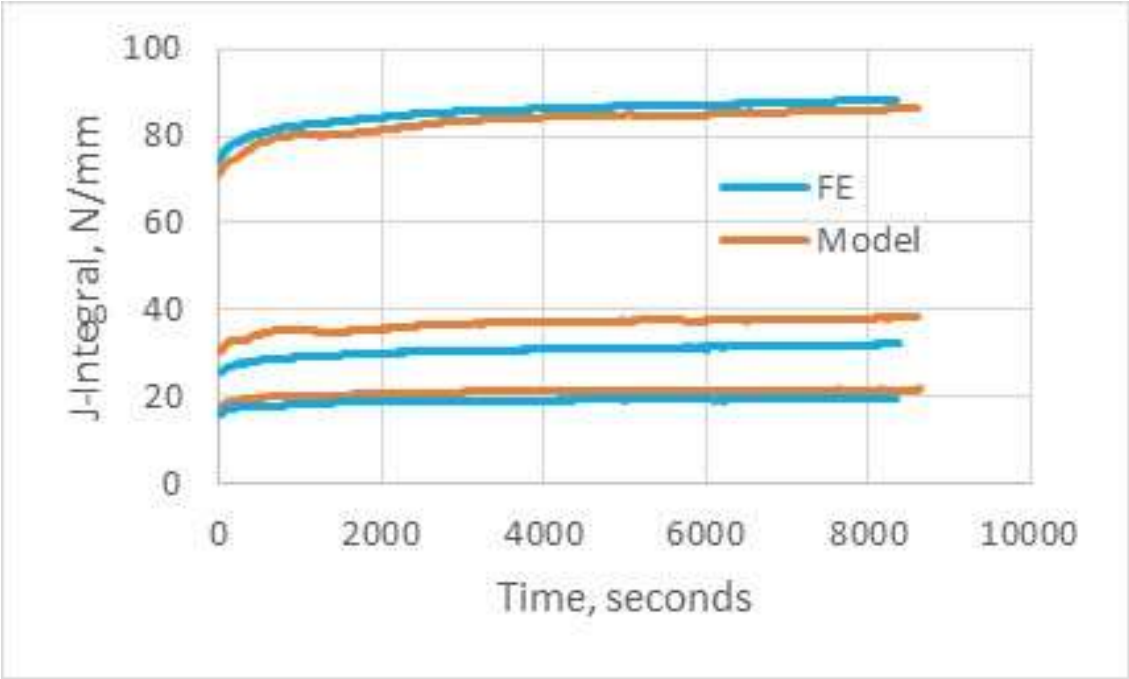


**Figure 7. Comparison of long-term J-integral values for a cracked center cracked panel at three levels (295.6, 322.7, 358.5 MPa)**

### *Fatigue Crack Growth*

All pipelines experience pressure cycles during their lifetime. Furthermore, virtually all older electric resistance weld (ERW) pipe is subjected to longitudinal seam cracking. As a consequence, the life and integrity of such ERW pipe, whether it contains cold welds, hook cracks, or selective seam weld corrosion (SSWC) will be driven by crack growth during operation. To estimate the damage that pressure cycles will induce in ERW pipe, a model for fatigue crack growth must be a part of the pipeline integrity repertoire.

The foundation of the fatigue model is standard fracture mechanics principles. That is, for a given crack/pipe geometry and pressure cycle: 1) the maximum and minimum stress intensity factors are calculated, 2) the calculated SIF's are modified to account for crack growth retardation due to overloads, and 3) an increment of crack growth is calculated which includes the effect of variations in stress-ratio and threshold effects. The effects of crack growth retardation, stress ratio and threshold are, typically, not considered in many pipeline fatigue applications. Accordingly, it is important to present the underlying theory and assumptions for these aspects of the present fatigue analysis problem because they do change predicted life, and sometimes, substantially.

If a time history of pressure has been turned into paired maximum and minimum pressure cycles using a cycle counting technique such as Rainflow cycle counting or the equivalent range-pair cycle counting [11], the paired maximum and minimum pressures are used to calculate the maximum and minimum stress intensity factors,

$$K = \sigma f(a, c, \ldots)\sqrt{\pi a} \tag{8}$$

where σ is an applied remote hoop stress, f is a crack geometry-specific factor (a function of part geometry, crack depth, crack length, crack location in the part, etc.), and a is the characteristic crack dimension (length or depth). The factor f changes for different types of cracks (cold weld, SSWC, embedded, through-wall), different crack geometries (depth-to-thickness ratio, length-to-depth-ratio, etc), and around the perimeter of a crack front (f at the tip of a surface crack differs from f at the deepest part of the surface crack).

The Task 3 report summarizes stress intensity factors for various ERW-specific flaw geometries.

Based on vast amounts of testing, it has been shown that regardless of the specific crack geometry, if two cracks in the same material have the same stress intensity factor range ($\Delta K = K_{max} - K_{min}$ corresponding to the stress intensity factor at maximum stress, $\sigma_{max}$, and minimum stress, $\sigma_{min}$, over a loading cycle), they will grow at the same rate and this growth rate will generically look like Figure 8 [12]. Typically, both growth rate and stress intensity factor range are plotted on log scales.

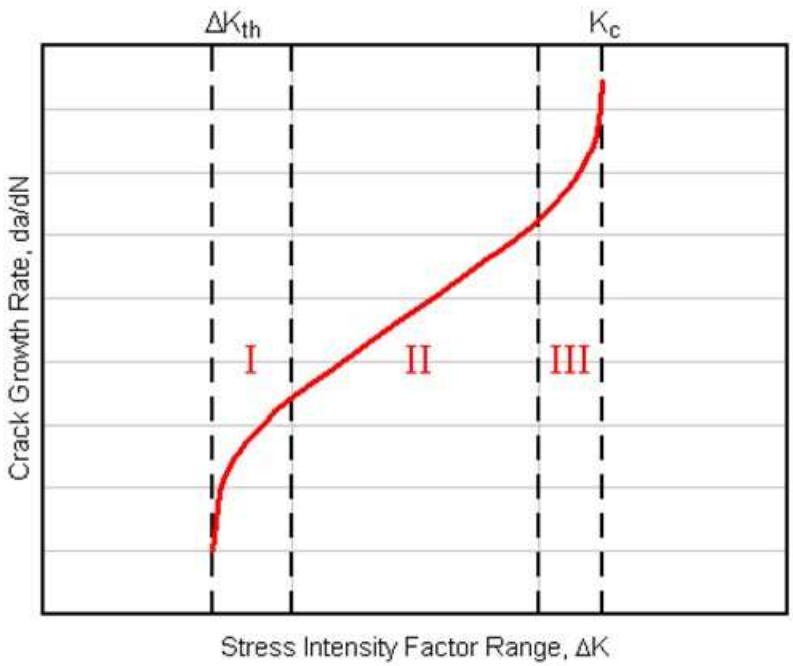


**Figure 8. Generic fatigue crack growth behavior [12]**

In Region I, crack growth is very slow. In fact, below some value of $\Delta K$, $\Delta K_{th}$, crack growth will be so small as to be undetectable. The growth behavior of most observable cracks is governed by Region II, where the growth rate is nearly linear on a log-log scale,

$$\frac{da}{dN} = C(\Delta K)^n \tag{9}$$

Material constants for C and n are routinely measured and published. Equation (9) is commonly referred to as the Paris Equation [13]. In Region III, rapid, unstable crack growth dominates as the part experiences the last few cycles of life. Region III is not really of interest for the present work.

The values of growth rate in Figure 8 are a function of:

- The environment. Crack growth rate is substantially different in a corrosive environment (stress corrosion cracking) versus a simple aqueous environment versus in air, versus in a hydrogen rich environment, etc.
- The stress ratio. Stress ratio is defined as

$$R = \frac{\sigma_{min}}{\sigma_{max}} \tag{10}$$

  Stress ratio can be negative (tension-compression) or positive (tension-tension) or zero (tension-unload to zero). Typically, R < 0 is no more damaging than R = 0. For the pipeline case, R is always positive.
- Frequency (Hz) of the loading.
- Specimen size, to some degree.
- Whether or not $\Delta K$ is above a minimum value, $\Delta K_{th}$, the so-called threshold $\Delta K$.

A simple model for crack growth that includes a threshold effect and stress ratio effect (using the Walker equation [9]) is,

$$\begin{aligned} \frac{da}{dN} &= C\left[\frac{\Delta K}{(1-R)^{1-m}}\right]^n, \qquad \Delta K > \Delta K_{th} \\ \frac{da}{dN} &= 0, \qquad \Delta K \leq \Delta K_{th} \end{aligned} \tag{11}$$

where $\Delta K_{th}$ is the threshold stress intensity factor ratio that is determined experimentally, R is the stress ratio, C, n, and m are material constants with $0<m\leq1$. When R>0, as m increases, the effect is to decrease the crack growth rate. In the limit as $m\rightarrow1$, Equation (11) degenerates to Equation (9). For a fixed value of m, as R increases, the crack growth

rate increases dramatically. Parameter m is determined by crack growth rate testing at various values of R.

In fatigue, an overload retards crack growth by forming a plastic zone that the crack must grow through before the growth rate returns to the original value. In the extreme, an overload can even completely arrest crack growth. Crack retardation might be explained by crack-tip blunting, compressive residual stresses at the crack tip, or crack closure effects. Figure 9 shows a schematic of how crack growth evolves before, during, and after an overload. Most retardation models base the magnitude of the effect on the Irwin plastic zone [14] [15] size in front of the crack

There are many retardation models, but one that seems to work well and that has been implemented in many crack growth models is the Willenborg model [10] . Effectively, Willenborg's model says that when an overload occurs at a crack that is subsequently relieved during unloading, a compressive stress field is generated in front of the crack tip. This compressive stress field reduces the effective stress on the crack tip so that the stress intensity factor is reduced. This is accomplished by substituting the maximum and minimum effective stresses for the actual stresses in Equation (9). For any applied load after an overload, as long as the current plastic zone lies within the plastic zone created during the overload, there will be a retardation effect consistent with Figure 10. With Willenborg's model, the retardation is maximum immediately after the overload and diminishes as the crack grows.

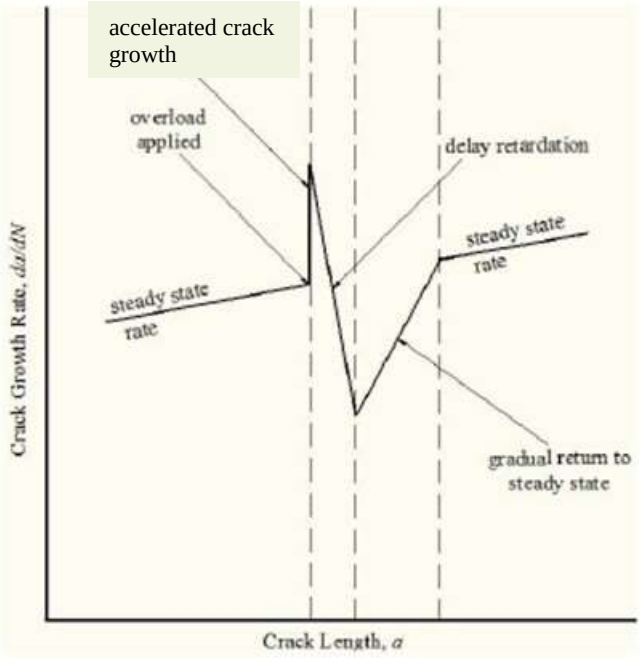


**Figure 9. Typical crack growth transients around an overload [10]**

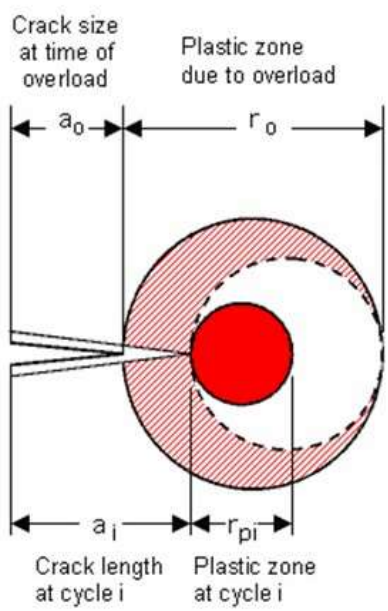


**Figure 10. Willenborg crack retardation model plastic zone [10]**

For the pipeline pressure cycle problem, crack retardation is an ongoing phenomenon. Starting from an overpressure, crack growth will be retarded until the crack has grown sufficiently that the current plastic zone touches the plastic zone created during the overpressure. After that, new plastic zone sizes will continue to be developed and overcome, depending on the loading.

Given that crack growth rate can be calculated at any given crack size, including the effects of retardation and stress ratio, the current crack size is the integral of the crack growth rate, Equation (11). Just as with growth in the depth direction, Equation (11) applies to growth in the length direction, so "a" is simply replaced by "c".

As a final note, it is important to point out that the Willenborg crack retardation discussion applies equally well to the material response during a hydrotest. That is, if the hydrotest pressure is sufficiently high with respect to operating pressure cycles, the hydrotest will induce a large plastic zone at the crack. In the best of circumstances, this plastic zone will be large enough that it will push the effective stress intensity factor range below $\Delta K_{th}$, thereby suppressing all subsequent fatigue crack growth for the life of the pipe. In the more usual circumstance, the hydrotest will reduce the crack growth rate to a level that a subsequent hydrotest will not be required to revalidate integrity for some years. Details of the model can be found in Reference [16]

# Validation

## Time-Independent Models

Data was obtained from various sources to conduct validation on the failure prediction models developed for PipeAssess PI™. While data was not available to test every model, one of the principles of fracture mechanics is the toughness parameters are formulated correctly for each of the models and the plastic collapse models are formulated correctly for each of the models, then the results should be comparable (i.e. similitude holds between specimens and structures). It should be noted that the pedigree for each of the datasets varies widely with respect to the know material properties. However, based on the results, the models are very accurate if all the material properties are known a-priori. The initial data set was obtained from Appendix E of NG-208 [17] and Reference [18]. The results of the analyses are shown in Figures 11 through 13. High

failure pressures are the results of small cracks which have higher variability in their size estimation. This variability in input is driving the higher variability in the output.

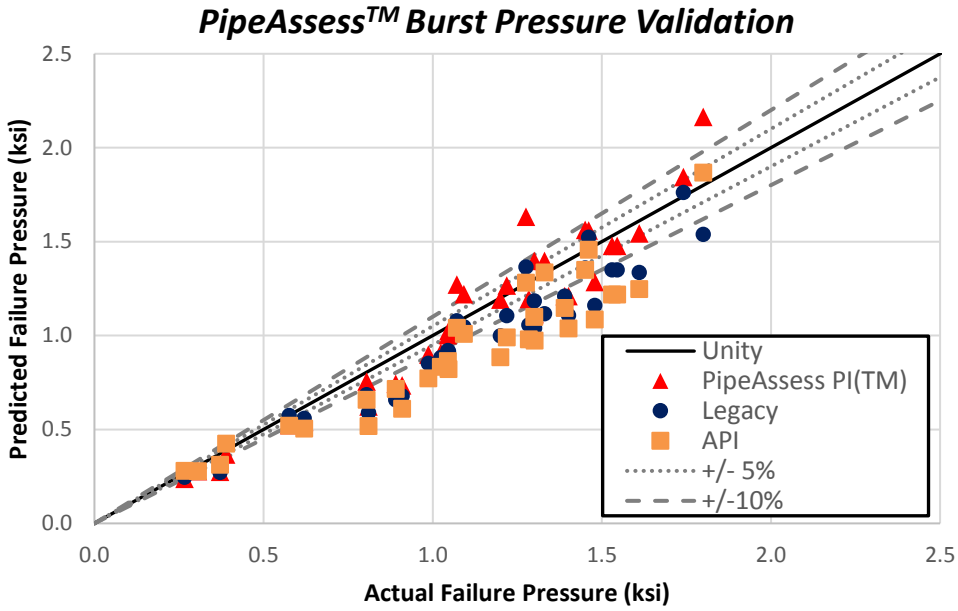


Figure 11. Failure pressure comparison using various models

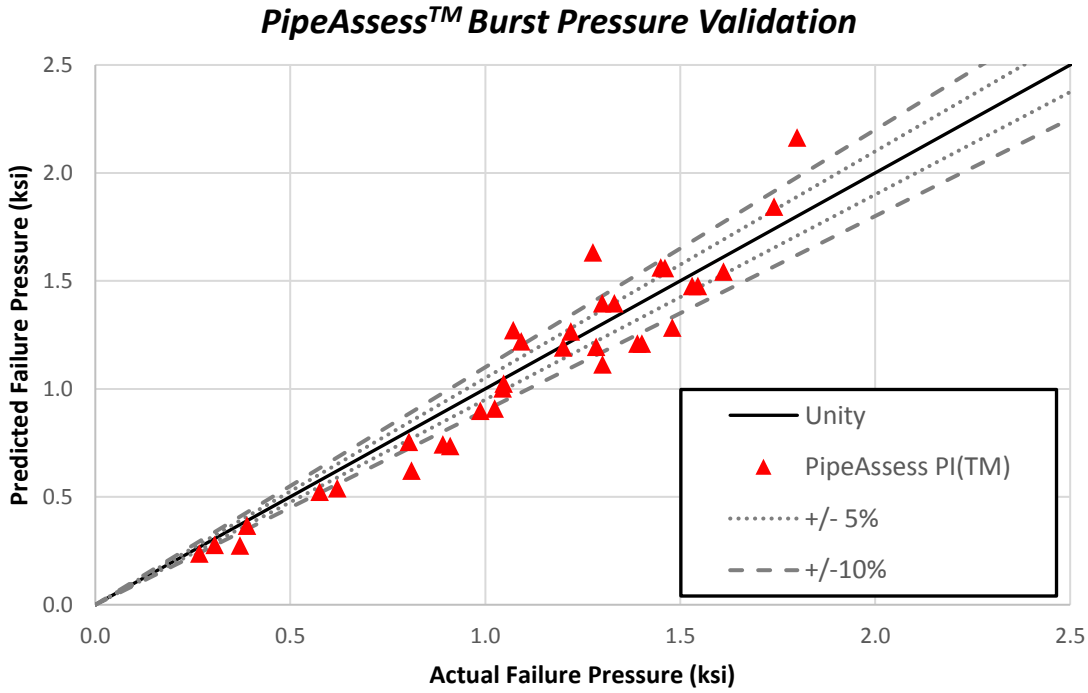


Figure 12. Failure pressure comparison for PipeAssess PI™ Only

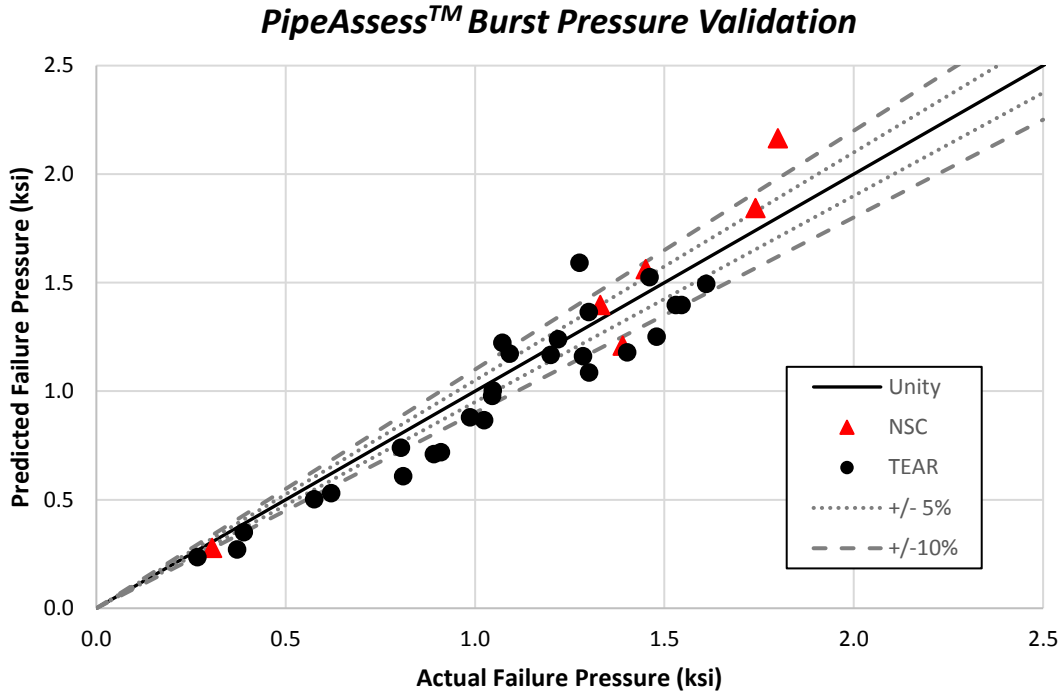


**Figure 13. Comparison of Tearing and Net-Section-Collapse (NSC) Results**

In the investigator's opinion, as shown in Figure 11, the results from PipeAssess PI™ are less conservatively bias than the other models and more accurately represent the mean value of the experimental data. All models exhibit similar variability between prediction and actual failure pressure which indicates the variability in the output is driven by the uncertainty in the input parameters.

*When data is not well defined such as data from Reference [19]* as shown in Figure 14, the variability in the results can be significant. The results obtained from this data used Yield Strength and Ultimate Tensile Strength data that was based on user experience, not actual data in the records. Additionally, historic Charpy values (8 – 12 ft-lbs) were used in place of actual Charpy data. While general trends can be determined (such that the data scatters about the unity line), the accuracy of the results are very dependent on the accuracy of the inputs.

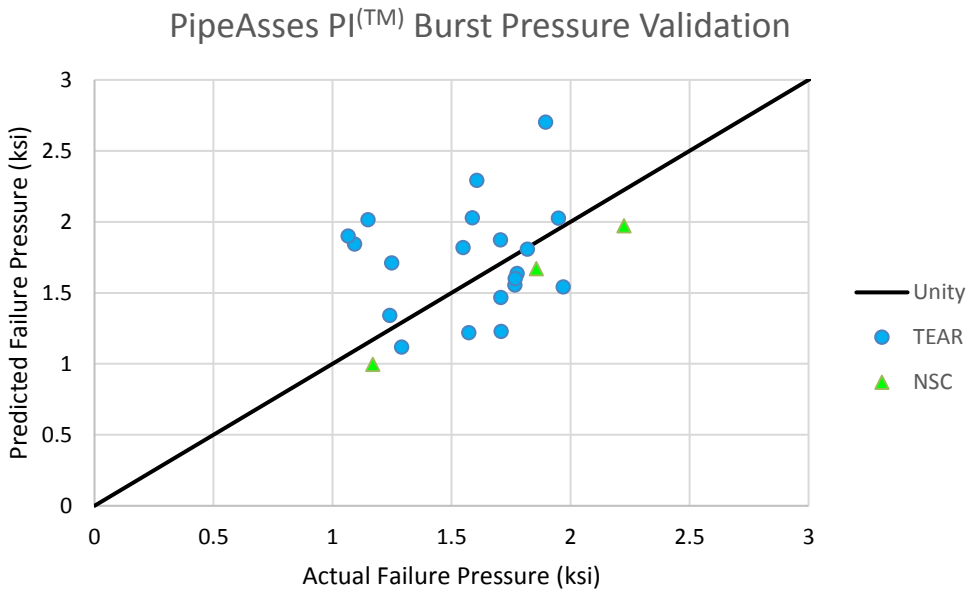


**Figure 14. Results using Data from Reference [19]**

In addition, Reference [19] also reviewed Hook Crack using Newman-Raju and Modified LnSec formulations. Figures 15 and 16 show the results of those analyses. Figure 17 shows the results of the analyses with the use of the new PipeAssess PI™ with the surface crack solution. It should be noted that for these cracks, *the necessary data was not available to model as true hook cracks [16]*. Both the material properties and the crack geometry were best estimates, not actual values. This lack of information drives significant variability in the results. As shown in Figure 17 (using all available data), the variability in the results can be significantly reduced using the updated stress intensity solutions. Also, for the analyses displayed in Figure 17, the CVN values were for the full-body pipe, not the local CVN values near the crack the "near crack" values were not available.

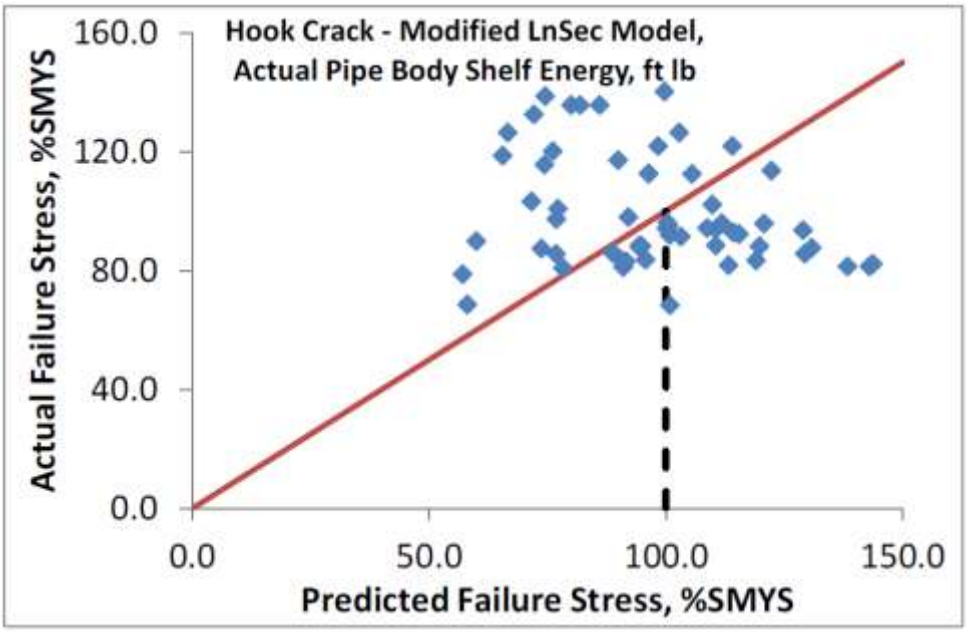


Figure 15. Results from Phase I, Task 2.4 [19]

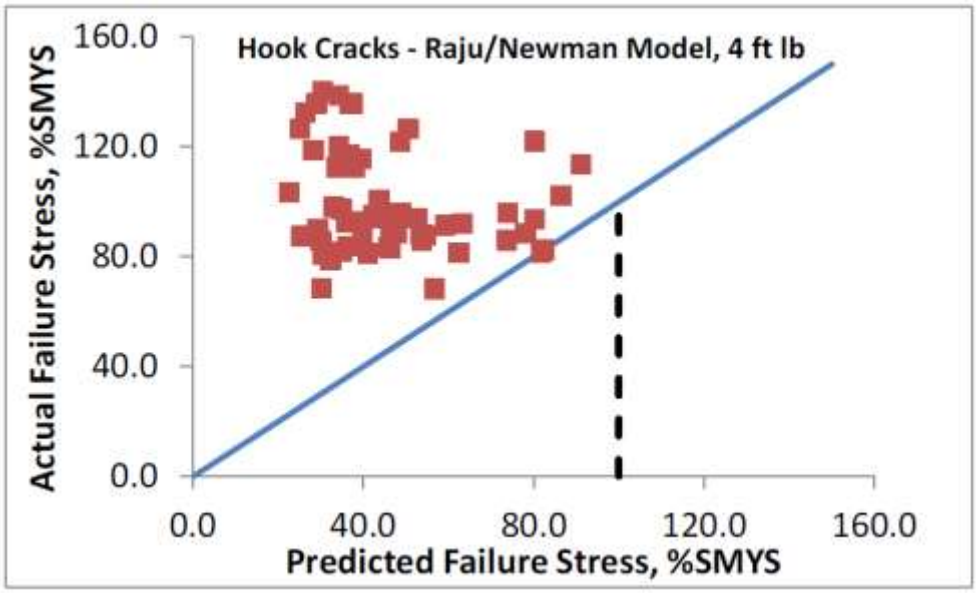


Figure 16. Results from Phase I, Task 2.4 [19]

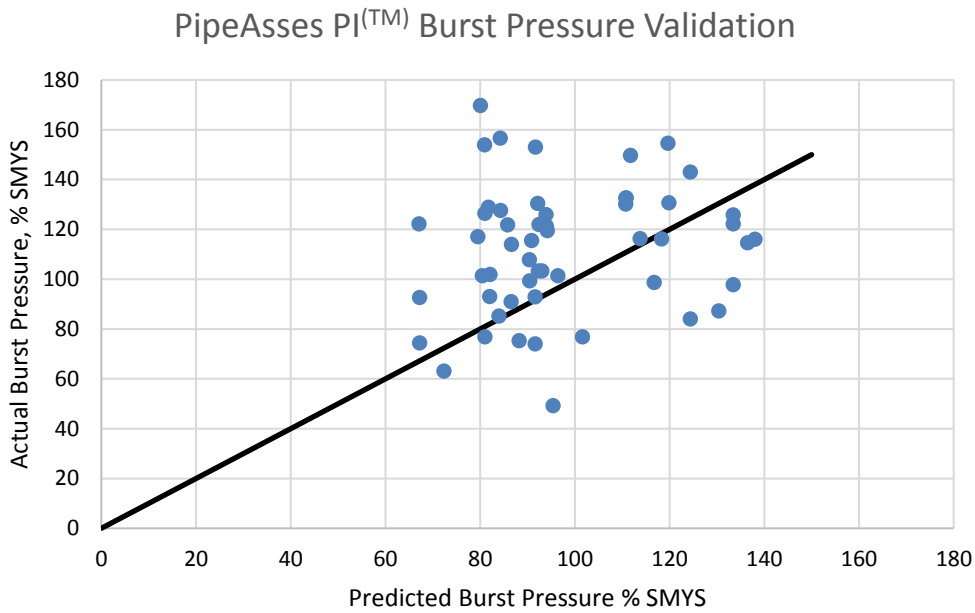


**Figure 17. Hook Crack Results using Cold Weld Analyses in PipeAssess PI™**

## Time-Dependent Models

### *Stress-Induced Creep*

The simplified engineering model for hydrotest time-dependent behavior has been applied to controlled pipe hydrostatic burst tests with artificial flaws to evaluate how it performs [7]. A 762 mm x 10 mm X52 pipe with the four flaws shown in Table 1 was pressurized per the loading shown in Figure 18.

**Table 1. Flaw set for stress-induced creep (hydrotest) model validation**

| FLAW # | DEPTH, A (mm) | LENGTH, 2C (mm) |
|---|---|---|
| 1 | 7.00 | 133.86 |
| 2 | 7.11 | 126.37 |
| 3 | 7.57 | 120.65 |
| 4 | 7.72 | 109.73 |

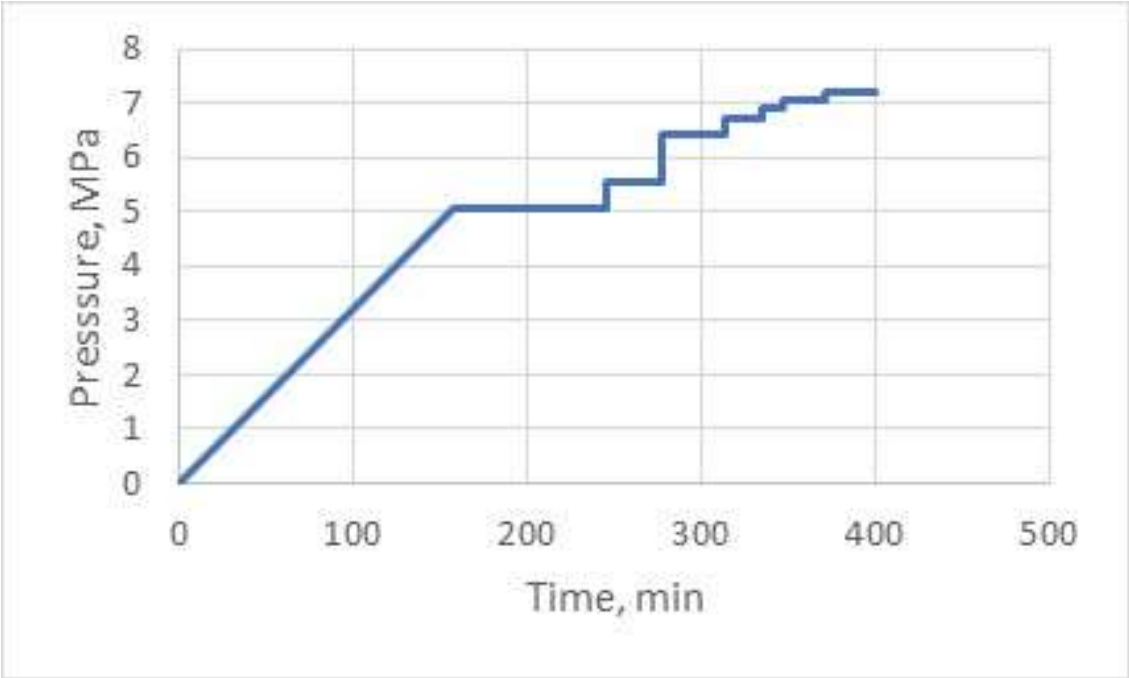


**Figure 18. Pressurization data for time-dependent growth hydrotest model validation**

Figure 19 through Figure 22 show comparisons between experimentally observed crack growth through the depth as estimated by d-c- electric potential measurements and crack growth predicted by the model. For Flaw 1 (Figure 19), the predictions are conservative, with crack initiation predicted earlier than the corresponding experimental results. The predicted final crack length is slightly conservative as is the failure pressure.

Significant crack growth occurs during the pressure hold periods, so neglecting time-dependent effects would be non-conservative. For Flaw 2 (Figure 20), the model under-predicts the amount of crack growth, but is conservative with respect to failure pressure. Considering Flaw 3 (Figure 21), the failure pressure and crack growth are both slightly conservative. Finally, for Flaw 4 (Figure 22) which had an instrumentation issue so that only the final crack size and failure pressure are known, the model yields slightly conservative predictions for failure pressure and crack growth.

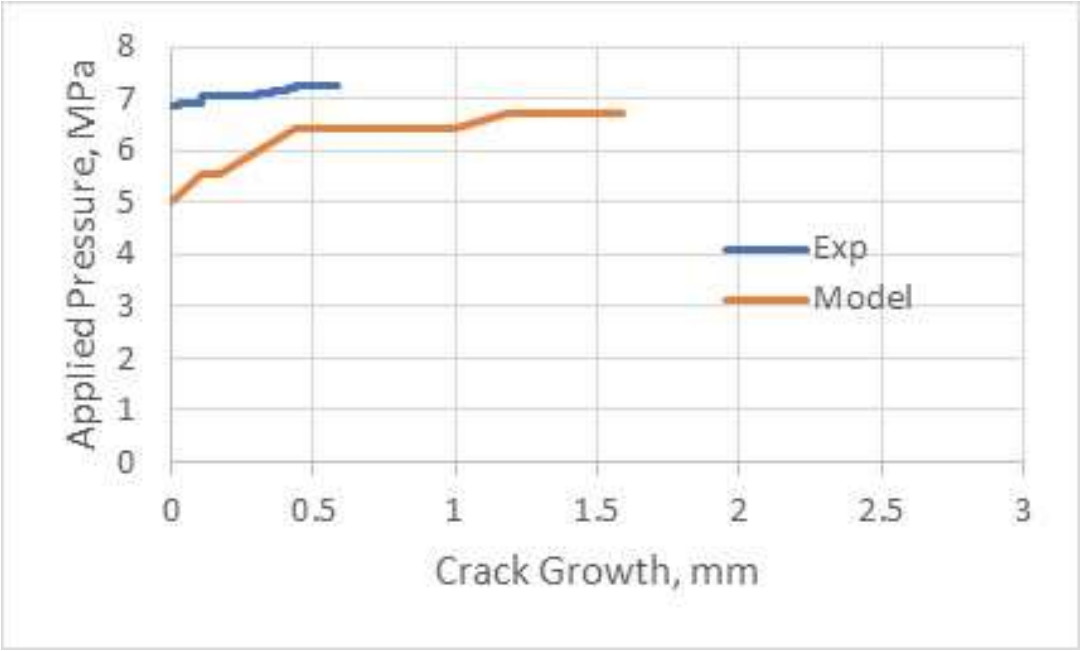


**Figure 19. Experimental (Exp) and model predicted time-dependent flaw growth for a 7.00 mm x 133.86 mm surface flaw in 762 mm x 10 mm X52 pipe**

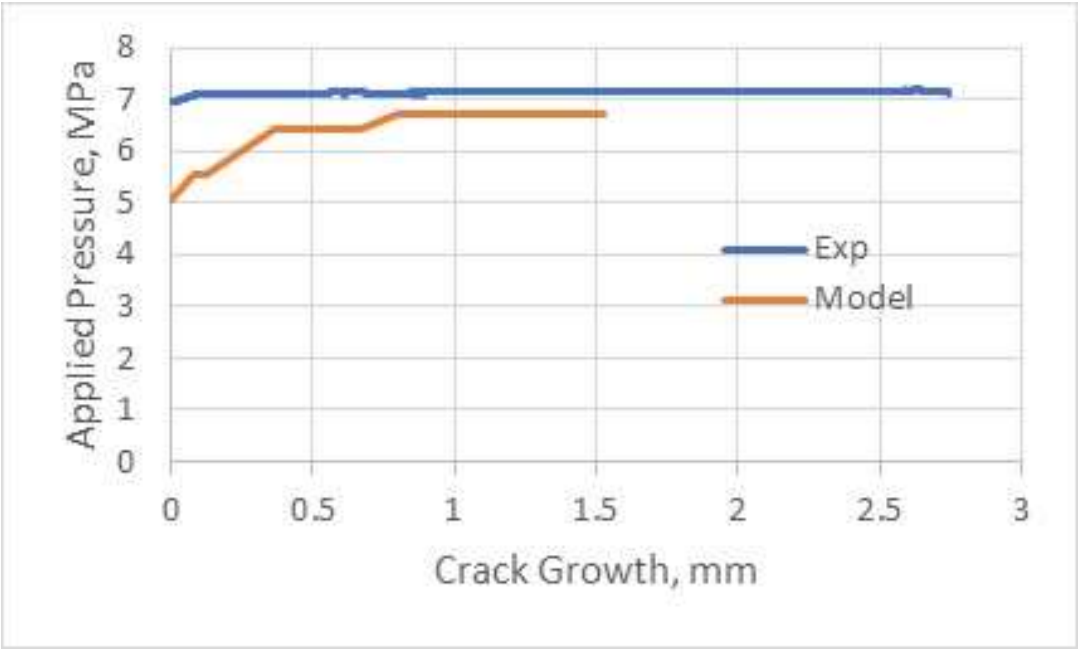


**Figure 20. Experimental (Exp) and model predicted time-dependent flaw growth for a 7.11 mm x 126.37 mm surface flaw in 762 mm x 10 mm X52 pipe**

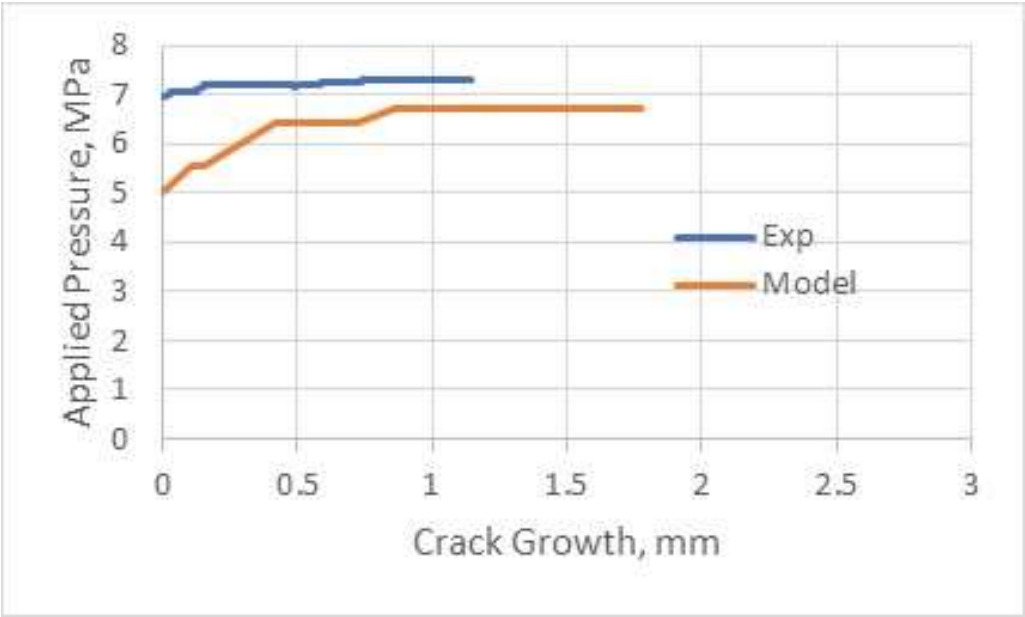


**Figure 21. Experimental (Exp) and model predicted time-dependent flaw growth for a 7.57 mm x 120.65 mm surface flaw in 762 mm x 10 mm X52 pipe**

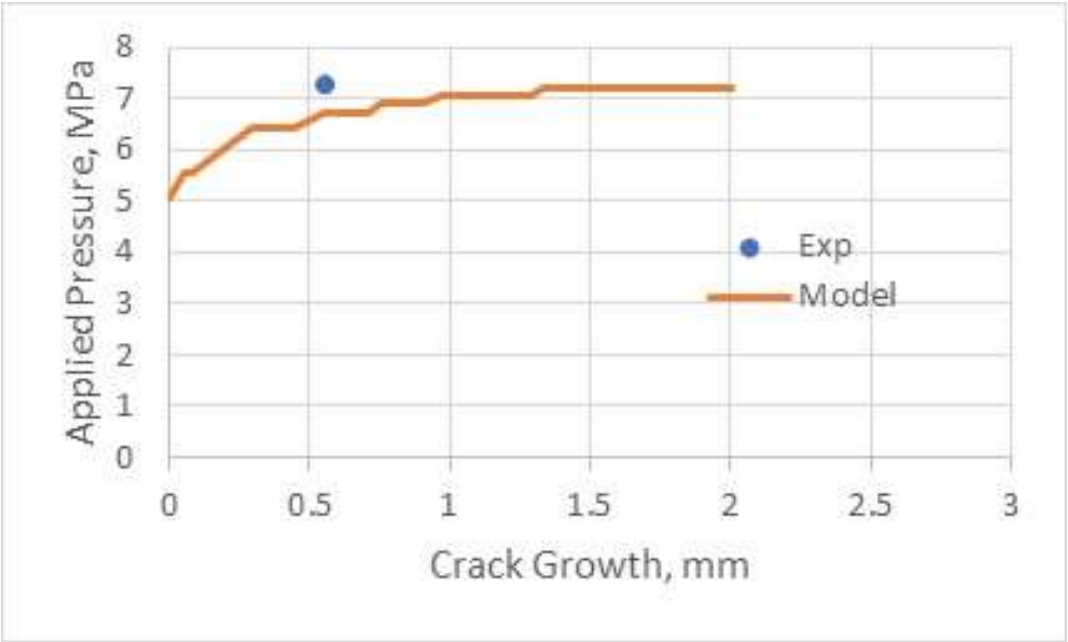


**Figure 22. Experimental (Exp) and model predicted time-dependent flaw growth for a 7.72 mm x 109.73 mm surface flaw in 762 mm x 10 mm X52 pipe**

*Fatigue*

Validation of the fatigue models used in the development of the software (Task 5) was conducted using two methods. Method 1 used ASTM E647 compact tension tests

with complex loading conditions to ensure the analytical models provided adequate results when compared to the test data. Examples of the applied stress intensity factors as a function of cycles are shown in Figure 23 and 24. Additional validation results can be found in Reference [16].

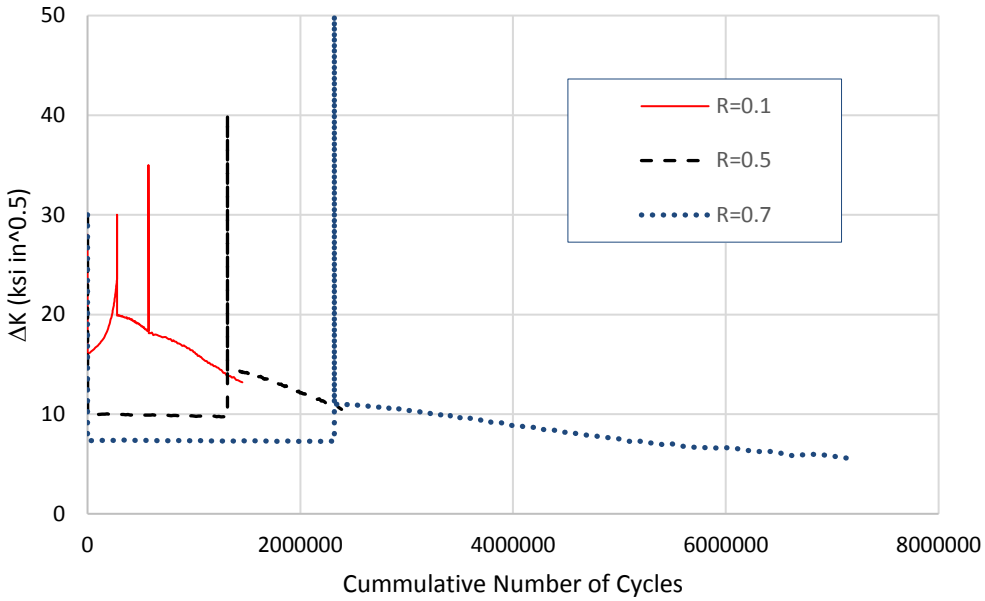


**Figure 23. Intensity Range Profiles for Grade B Tests with various stress ratios (R)**

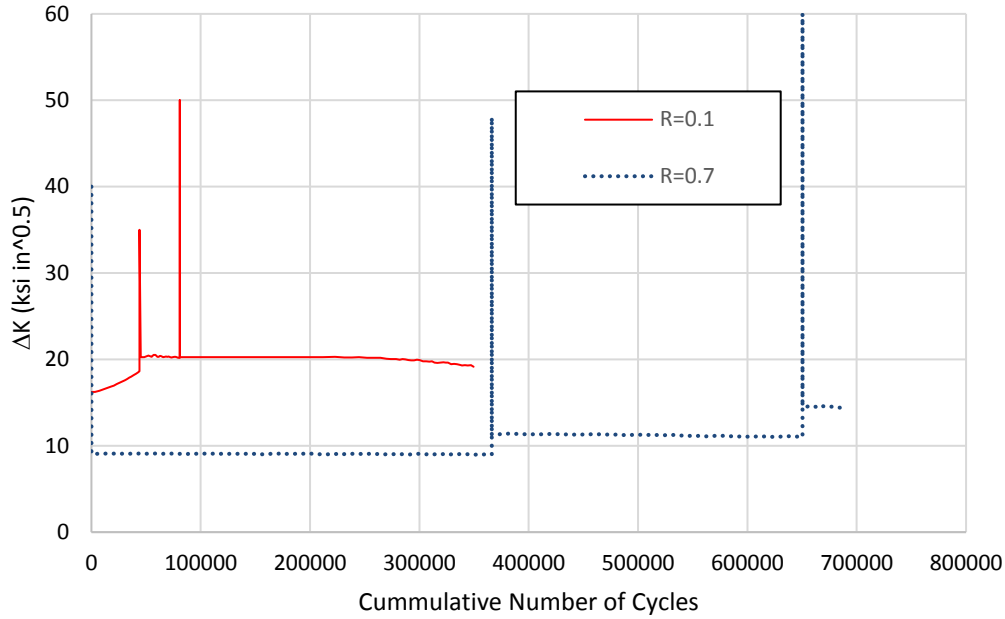


**Figure 24. Intensity Range Profiles for Grade X-70 Tests with various stress ratios (R)**

Based on the test results, Figure 25 an 26 provide the results of the validation of the models. A unity plot was used to show the validation.

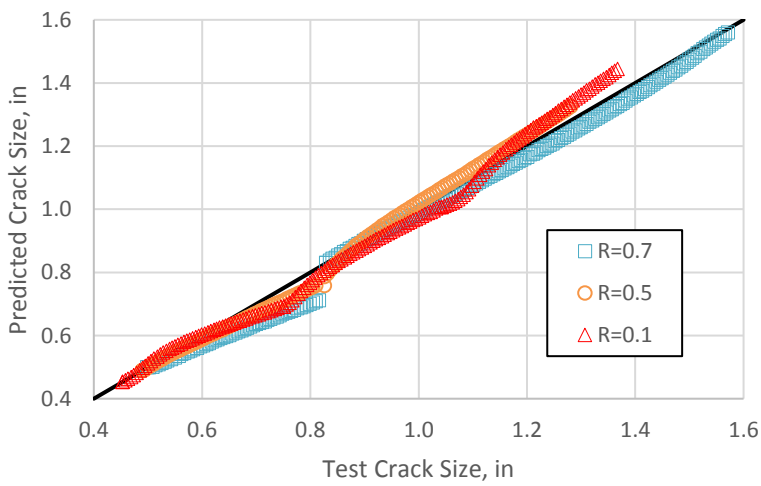


**Figure 25. Unity Plot for Crack Sizes of the Grade B Tests with various stress ratios (R)**

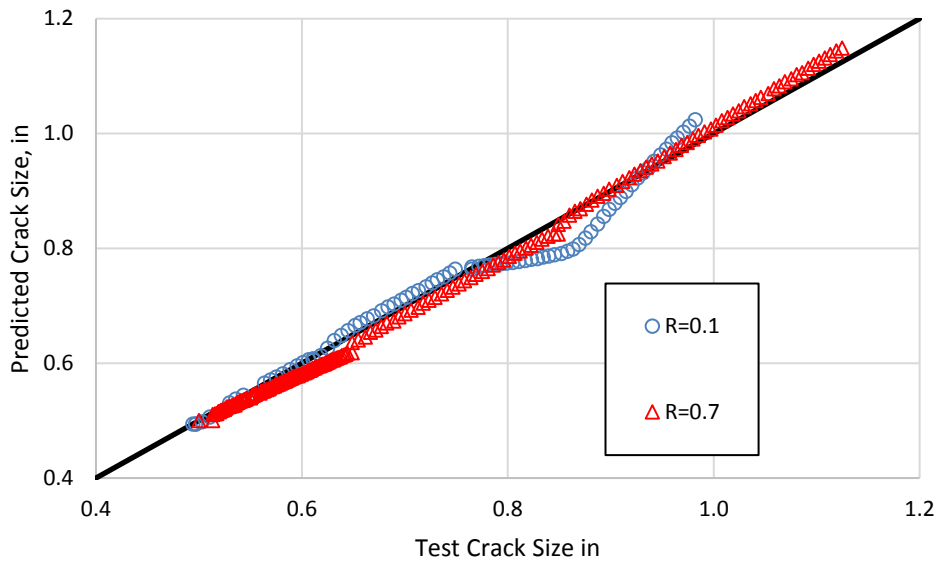


**Figure 26. Unity Plot for Crack Lengths of the X-70 Tests with various stress ratios (R)**

Validation method 2 used full-scale pipe fatigue tests with artificial axial cracks inserted via an electric discharge machining technique. In this validation effort, four semi-elliptical axial cracks with different depths and lengths were introduced into a length of pipe. The flaws were then pressure cycled to grow them. After a number of cycles were applied, the flaws were cut out of the pipe, cold cracked, and visually examined under magnification to compare predicted crack growth using PipeAssess PI™ with observed crack growth.

### *Full-Scale Fatigue Test: Experiment Design*

The goals for designing the experiment were:

1. Select a specimen configuration from a full-sized pipe that can be physically handled without the use of lifting equipment
2. Select a pressure cycle range that does not subject the specimen(s) to more than 80% SMYS maximum stress
3. Design the specimen(s) so that multiple flaws can be tested simultaneously
4. Select a pipe size and flaw sizes that result in leakage of the largest flaw in a reasonable number of cycles (<100,000 cycles)
5. Control as many variables as possible to minimize scatter in the data.

Using PipeAssess PI™ analyses with an assumption of an API-579 external surface crack K solution, the following specimen configuration was employed with the listed material properties:

- Pipe Stock: 6-inch Sch 40, A53-B pipe (6.625" OD, 0.280" wt)
    - Gr B, $\sigma_u$=60 ksi, $\sigma_y$=35 ksi
    - CVN<30 ft-lb
- Pipe OD/ID turned to 6.57" OD, 0.16" wt
- Pipe length: 12-inches
- Pressure cycles: 120 psi to 1200 psi (68% SMYS)
- Flaws – all semi-elliptical, introduced using a shaped plunge EDM cutter, spaced at 90-degrees, in the middle of the length of the specimen:
    - 0.040" deep x 0.800" long (calculated that the flaw will leak at approximately 83,900 cycles)
    - 0.016" deep x 2.000" long (flaw will grow in depth but not length)
    - 0.066" deep x 0.132" long (flaw will grow in depth and length)
    - 0.016" deep x 0.250" long (flaw will not grow in depth or length).

With this design, Goal 1 is satisfied because the specimens can easily be lifted by hand. Design Goal 2 is met by only applying pressures up to 1200 psi. Four flaws satisfy Goal 3 and less than 100,000 cycles predicted to leakage of one flaw satisfies Goal 4. Goal 5 is satisfied by: 1) turning the OD and ID, 2) by starting with initial flaws that have the natural equilibrium shape when they grow, and 3) using a unique test apparatus configuration to eliminate pipe ends effects (discussed below).

### *Test Apparatus*

Like any typical fatigue test, applying load cycles rapidly is desirable to limit test machine time. For these tests, a unique test setup was selected. Traditionally, pipe specimen fatigue tests are conducted by repeatedly filling and draining a long specimen. The long specimen is used to get the test flaws away from reinforcing end cap effects. Draining of the specimen is usually accomplished using only the elasticity of the pipe body to force the pressurizing fluid out of the specimen. Diminishing driving force as the pressure in the specimen drops, compressibility of the test fluid, and flow losses in

fittings, hoses and valves make it difficult to get to near ambient pressures. Setting the lower pressure much higher than ambient reduces the driving stress intensity factor range that governs fatigue crack growth, causing the tests to take much more time.

As an alternative to the fill/drain style of pressure cycling on a long specimen, this test program selected a rather different approach:

- A relatively short specimen with floating end caps restrained axially with tie rods that eliminate the need for welded end caps. Seals on the floating end caps provide pressure integrity.
- A hydraulic actuator inside the specimen. Extension and retraction of the actuator rod displaces fluid, increasing and decreasing the specimen internal pressure.
- Filling the bulk of the internal cavity of the specimen with a volume absorber to minimize the amount of working fluid.

Figure 27 shows a section view of the test setup.

As illustrated in Figure 27, four tie rods carry the axial "end cap" load. The end caps have elastomeric seals interposed between a shoulder on the end cap and the pipe specimen ID to make the specimen leak tight. A double-acting hydraulic actuator inside the specimen extends and retracts, displacing fluid and raising/lowering the internal pressure. The actuator, in this case, actively "pulls" back instead being pushed back by the elasticity of the specimen, so the decrease in pressure can be as rapid as the pressure increase (so long as the actuator is not pulled back so fast that the fluid boils). The hydraulic actuator, a work holding cylinder, gets hydraulic connections to outside of the end cap via O-ring face seal fittings and JIC 37-degree fittings. A pressure transducer and pressure relief device are plumbed to the interior of the specimen using standard NPT fittings. Finally, and not shown for clarity, the specimen is filled with glass beads. The glass beads are orders of magnitude less compressible than the working fluid, water, so the actuator stroke to achieve a given specimen pressure is greatly reduced. Screen guards keep the beads away from the actuator and pipe ID. Figure 28 through Figure 31 show pictures of the test setup and the external image of one of the test cracks.

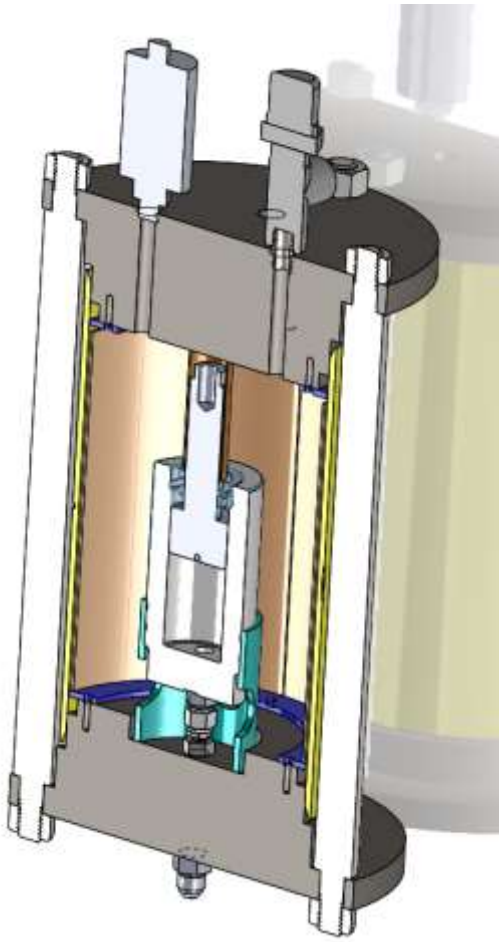

**Figure 27. Cross Section of the Test Apparatus**

**Figure 28. Picture of the Bottom Head and Hydraulic Actuator**

Figure 29. Picture of a Typical Test Flaw

**Figure 30. Picture of the Assembled Specimen**

Figure 31. Picture of the Specimen and Servo-Hydraulic Test Control System

Not shown in Figure 27 are connections from the actuator fittings on the end cap to a hydraulic servo-valve that is controlled by a programable MTS servo-controller. Typical tensile test laboratory hydraulic power supply and hydraulic service manifold hardware completes the system. Feedback for the closed-loop servo-system is via the pressure transducer.

Operationally, with one head off, the specimen is filled with water, then beads are added making sure that the beads are free of air bubbles. When the specimen is full, the second head is installed, and the tie rods secured. Multiple cycles of vacuum degassing/filling are applied to eliminate all air from inside the system. Once the system has all air removed, the servo-control computer is programmed with the mean pressure

value, the desired pressure amplitude, and the cycle frequency. The actuator is then extended manually under servo-control to the mean value of the pressure cycle and the program executed. Limit detects in the servo-control software are set to the that when the specimen leaks and the actuator cannot make the commanded maximum pressure, the system automatically shuts down.

*Results*

Table 2 lists the pressure ranges and number of cycles applied to the test specimen. A post-test pictures of the flaws are shown in Figure 32 to 36. In these figures, the initial EDM notches are clearly visible as is any crack growth from the applied pressure cycles. Table 3 lists the predicted crack growth and measured crack growth for the flaws.

**Table 2. Pressure Cycles Applied to Specimen**

| Pmax, ksi | Pmin, ksi | Cycles |
|---|---|---|
| 1.192 | 0.257 | 1,200 |
| 1.300 | 0.373 | 3,800 |
| 1.350 | 0.427 | 1,978 |
| 1.350 | 0.350 | 15,300 |
| **Total** | | 22,278 |

**Table 3. Predicted and Actual Crack Growth**

| Specimen | Initial Flaw Size, inches | | Change in Size, Predicted, inches | | Change in Size, Actual, inches | |
|---|---|---|---|---|---|---|
| | Depth | Length | ΔDepth | ΔLength | ΔDepth | ΔLength |
| 1 | 0.066 | 0.132 | 0.001 | 0.006 | 0.000 | 0.000 |
| 2 | 0.040 | 0.800 | 0.006 | 0.000 | 0.0046 | 0.000 |
| 3 | 0.016 | 2.000 | 0.000 | 0.000 | 0.000 | 0.000 |
| 4 | 0.016 | 0.250 | 0.000 | 0.000 | N/A | N/A |

Figure 32. Specimen 1 – No Fatigue Indication

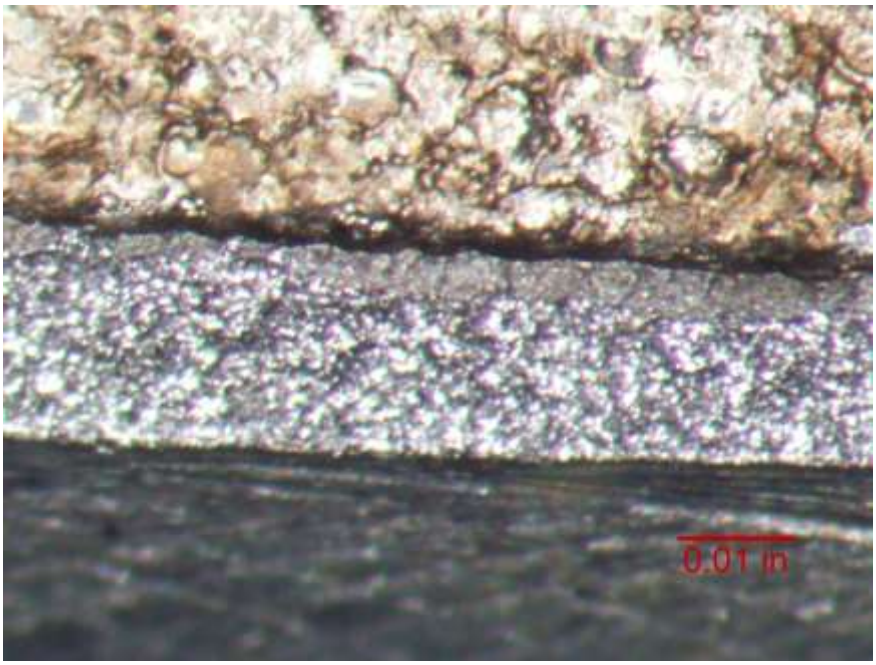


Figure 33. Specimen 2 – Fatigue Indication at Deepest Location

**Figure 34. Specimen 2 – No Fatigue Indication at Surface Location**

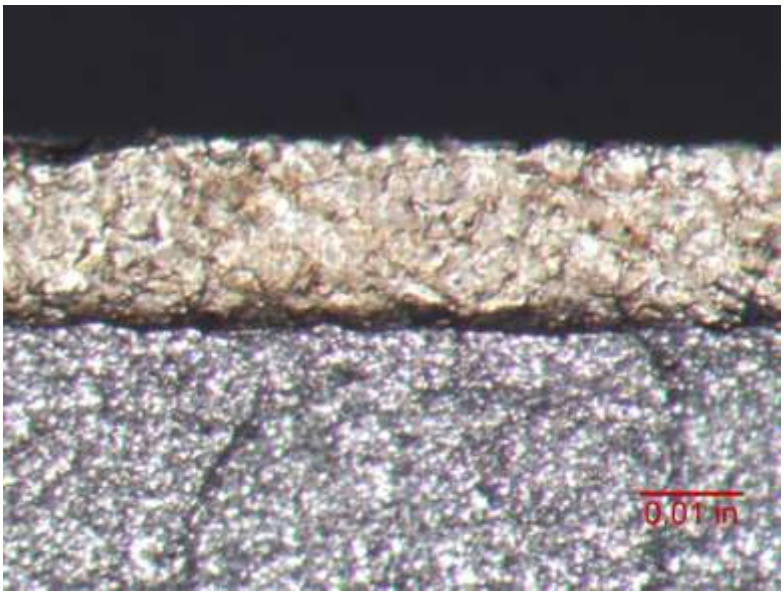


**Figure 35. Specimen 3 – No Fatigue Indication at Deepest Location**

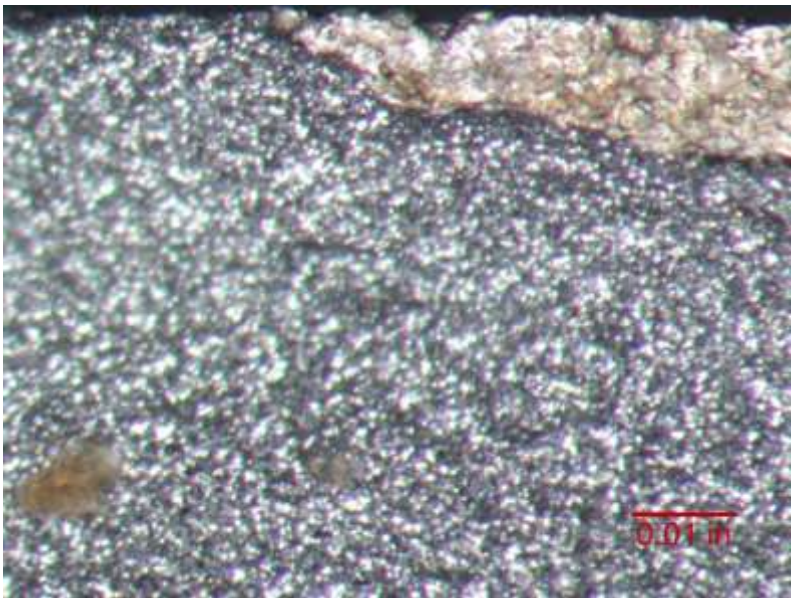


Figure 36. Specimen 3 – No Fatigue Indication at Surface Location

Based on the results of the full-scale fatigue study, the fatigue crack growth rate predictions appear to be conservative with respect to growth rate. In addition, incubation time to form a fatigue crack from an EDM flaw may have influenced the results. It is recommended that the additional testing be performed on full-scale pipe to determine the amount of conservatism in the calculations.

## Conclusions and Recommendations

The following conclusions and recommendations are provided based on the results obtained via validation.

- Analytical models were used based on historical literature information.
- New stress-intensity solutions, based on fracture mechanics theory, were developed using FEA in Task 3 and implemented in the software for Task 5. Task 4 focused on the validation of the implementation of the models.
- Net-section collapse and fracture-based tearing models were validated to historical full-scale test results.
- Stress-Induced creep models were validated based on historical data.
- Analytical fatigue models were validated based on both laboratory and full-scale tests

- Variability and Accuracy of inputs into the failure calculations significantly effects the outputs, thus
    - safety factors on output should be commensurate with the pedigree of the data used to generate the results
    - the best data availability should be used in the calculations (i.e. the local properties in the location of the crack; bond line, heat-affected zone, Body…etc.)
    - if known data is not availability, conservative assumptions should be made to ensure conservative calculations

- Hook-Crack analyses are challenging
    - embedded hook cracks should be analyzed with methodology as described in reference [16] embedded flaws
    - surface-breaking hook crack should be analyzed using the infinitely long surface crack with the appropriate Charpy energy

- In the investigator's opinion, as shown in Figure 11,
    - PipeAssess PI™ results are less conservatively bias than the other models
    - PipeAssess PI™ results more accurately represent the mean value of the experimental data
    - PipeAssess PI™ results show similar variability between prediction and actual failure pressure to other methods (Legacy and API)
    - the similarity in the variability in the output, for all the models shown, comes from the uncertainty in the input parameters

## Works Cited


[1] A. Willoghby and T. Davey, "Plastic Collapse in Part-Through Falws in Plates," in *Fracture Mechanics: Perspectives and Directions (Twentieth Symposium), ASTM STP 1020*, Philadelphia, 1989.

[2] The American Society of Mechanical Engineers and the American Petroleum Insititute, "API 579-1/ASME FFS-1, Second Edition," 2016.

[3] BSI Publications, "Guide to Methods for Assessing the Acceptability in Flaws in Metallic Structures, BS7910," 2013/2015.

[4] B. Leis and D. Stephens, "An Alternative Approach to Assess the Integrity of Corroded Line Pipe - Part One: Current Status and Part Two: Alternative Criterion," in *7th International Conference on Offshore Pipelines and Polar Engineering*, Lisbon, Portugal, 2007.

[5] D. Stephens, B. Leis, M. Kurre and D. Rudland, "Development of and Alternative Failure Criterion for Residual Stength of Corrosion Defects in Moderate-to-High-Toughness Pipe," PRCI Catalog L51794, 1999.

[6] W. Ramberg and W. Osgood, "Description of Stress-Strain Curves by Threee Parameters," Technical Note No. 902, National Advisory Committee for Aeronautics, Waschington, DC, 1943.

[7] B. Leis, F. Brust and P. Scott, "Development and Validation of a Ductile Flaw Growth Analysis for Gas Transmission Line Pipe," PRCI Catalog L51643, 1991.

[8] V. Kuhnle and H. Reidel, "Time-Dependent Deformation and Fracture of Stell between 20C and 400C," *International Journal of Fracture*, vol. 34, pp. 179-194, 1987.

[9] K. Walker, "The Effect of Stress Ratio During Crack Propagation and Fatigue for 2024-T3 and 7075-T6 Aluminum," in *Effect of Environment and Complex Load History on Fatigue Life: ASTM STP 462*, West Conshohocken, PA, 1970.

[10] J. Willenborg, R. Engle and H. and Wood, "A Crack Growth Retardation Model Using an Effective Stress Approach; AFFDL-TH-71-1-FBR," Air Force Flight Dynamics Laboratory, Wright Patterson Air Force Base, 1971.

[11] ASTM International, "Standard Practice for Cycle Counting in Fatigue Analyses: ASTM E1049-85(2011)," West Conshohocken, PA, 2011.

[12] Rolfe S. and J. Barson, Fracture and Fatigue Control in Structures, Englewood: Prentice-Hall, 1977.

[13] P. Paris and F. Erdogan, "A Critical Analysis of Crack Propagation Laws," *Journal of Basic Engineering, Transactions of the American Society of Mechanical Engineers*, pp. 528-534, 1963.

[14] G. Irwin, "Linear Fracture Mechanics, Fracture Transition, and Fracture Control," *Engineering Fracture Mechanics*, vol. 1, no. 2, pp. 241-257, 1968.

[15] G. Irwin, "Plastic Zone Near a Crack Tip and Fracture Toughness," in *Sagamore Ordinance Materials Conference*, Syracuse, 1961.

[16] B. A. Young, R. Olson and J. O'Brian, "Validation of Fatigue Models for ERW Seam Weld Cracking (Phase II, Task 3)," in *ASME PVP 2017*, Waikoloa, 2017.

[17] B. N. Leis and R. J. Eiber, "Fracture Control Technology for Transmission Pipelines (NG-18 208 Update)," Battelle Memorial Institute, Columbus, 2009.

[18] J. F. Kiefner, W. A. Maxey, R. J. Eiber and A. R. Duffy, "Failure Stress Levels of Flaws in Pressurized Cylinders," *ASTM STP 536*, pp. 461-481, 1973.

[19] J. F. Keifner and K. M. Kolovich, "Models for Predicting Failure Stress Levels for Defects Affecting ERW and Flash-Welded Seams," KAI, Worthington, 2013.

[20] B. A. Young, J. M. O'Brian and R. J. Olson, "Defect Characterization: Types, Sizes, Shapes, and Idealizations," Battelle Memorial Institute, Columbus, 2017.